PAPER • OPEN ACCESS

Synthesizability of transition-metal dichalcogenides: a systematic first-principles evaluation

To cite this article: Tenglong Lu *et al* 2023 *Mater. Futures* **2** 015001

View the article online for updates and enhancements.

Synthesizability of transition-metal dichalcogenides: a systematic first-principles evaluation

Tenglong Lu[1,2] ®, **Yanan Wang**[1,3], **Guanghui Cai**[1,2], **Huaxian Jia**[1,2] ®, **Xinxin Liu**[1], **Cui Zhang**[1,2,*], **Sheng Meng**[1,2,3,*] **and Miao Liu**[1,3,4,*] ®

[1] Beijing National Laboratory for Condensed Matter Physics and Institute of Physics, Chinese Academy of Sciences, Beijing 100190, People's Republic of China
[2] School of Physical Sciences, University of Chinese Academy of Sciences, Beijing 100049, People's Republic of China
[3] Songshan Lake Materials Laboratory, Guangdong 523808, People's Republic of China
[4] Center of Materials Science and Optoelectronics Engineering, University of Chinese Academy of Sciences, Beijing 100049, People's Republic of China

E-mail: cuizhang@iphy.ac.cn, smeng@iphy.ac.cn and mliu@iphy.ac.cn

Abstract

Transition metal dichalcogenides (TMDs) are a class of materials with various useful properties, and it is worthwhile to have a thorough evaluation of the characteristics of the TMDs, most importantly, their structural stability and exfoliability, in a systematic fashion. Here, by employing high-throughput first-principles calculations, we investigate the vast phase space of TMDs, including 16 bulk phases and 6 monolayer phases for all possible TMD combinations [comprising (3d, 4d, 5d) transition-metal cations and (S, Se, Te) anions], totaling 1386 compounds. Through the 'bird-view' of the as-large-as-possible configurational and chemical space of TMDs, our work presents comprehensive energy landscapes to elucidate the thermodynamic stability as well as the exfoliability of TMDs, which are of vital importance for future synthesis and exploration towards large-scale industrial applications.

Supplementary material for this article is available online

Keywords: transition metal dichalcogenides, high-throughput calculations, stability, exfoliability

1. Introduction

Transition metal dichalcogenides (TMDs) with the stoichiometry of TX_2 (T = transition metals, X = chalcogens) possess various appealing characteristics and cover a large polymorphic phase space. Composed of basic building blocks of octahedral (T), trigonal prismatic (H), and distorted octahedral (T′) coordinations, the layered TMDs can be stacked into various configurations including 1T, 2H, 3R, and 1T′ phases [1]. Experimentally, the single- or few-layered TMDs have been successfully synthesized through exfoliation to further expand the configurational phase space of TMDs [2, 3]. TMDs have many novel physical properties and enable various useful applications. For example, when the thickness of layered MoS_2 with the 2H polymorph shrinks down to monolayer, the film exhibits an indirect-direct band gap transition, which can be manifested via the enhanced photoluminescence in monolayer MoS_2 [4]. In addition, the finite but opposite Berry curvatures at K and K′ valleys in the Brillouin zone of

Future perspectives

Transition metal dichalcogenides (TMDs) are materials with abundant structural polytypes and novel physical properties. Previous research has focused on the synthesizability of single- or few-layer TMD compounds, but the polymorphic phases of TMD compounds have never been investigated at a 'bird view' level. This paper aims to evaluate the synthesizability and exfoliability of TMDs in a systematic fashion, providing a quantitative understanding of materials synthesis-structure relationships for TMDs across nearly all possible crystalline phases from layered to non-layered structures. This research is expected to be of great importance to the nanomaterials community.

monolayer MoS_2 make it a viable model material to investigate the behavior of valley electrons, such as the valley Hall effect [5]. In layered TMDs, alkali metal can intercalate into the interlayer spacing, enabling their applications for Li-ion and K-ion batteries [6]. Recently, the ultrathin TMDs start to rival the traditional silicon electronics technology for their superior carrier mobility when the feature size goes down below 2 nm [7]. The TMDs have many non-layered phases too, such as the pyrite-, marcasite-, and spinel-type structures, with widespreading applications in photovoltaics, photodetectors, and photoelectrochemical devices [1, 8–10]. In short, TMDs are indeed a family of useful materials with abundant polymorphic phases and various exotic properties.

Despite their rich polymorphic phases, TMDs are usually studied individually. From the thermodynamic point of view, the likelihood for a compound to exist is primarily determined by its standard enthalpy of formation, which is a measure of the energy released or consumed when one mole of a substance is created under standard conditions from its pure elements. A larger standard enthalpy of formation (more energy released during formation) leads to better stability of a compound. In many previous works, phonon spectroscopy has been employed to justify the stability of compounds, but the phase competition between polymorphs has been overlooked. Hence, the dynamically stable phases instead of thermodynamically stable phases of compounds were identified. However, many compounds, which are predicted or studied solely from phonon spectroscopy, are not necessarily synthesizable in the real world if they are not thermodynamically stable.

In order to fully understand the synthesizability of TMDs, the present work strives to chart a comprehensive map of formation enthalpy for TMD compounds with the stoichiometry of TX_2. On one hand, all possible polymorphic crystal structures of TMDs in the Inorganic Crystal Structure Database (ICSD) as well as the Atomly materials database [11, 12], totaling 1008 bulk and 378 monolayer configurations in 16 bulk polytypes (12 layered and 4 non-layered polytypes) and 6 monolayer polytypes, have been covered to obtain a comprehensive energy landscape. As a result, a complete configurational space of TMDs is covered, and their thermodynamic phase preference can be extracted correctly without missing any possible stable phases. On the other hand, the formation enthalpies of TMDs are obtained based on high-throughput density functional theory (DFT) calculations with the identical standard,

therefore their energies are mutually comparable. This work provides comprehensive energy landscapes for TMD compounds with the stoichiometry of TX_2 to justify their synthesizability and exfoliability once and for all.

2. Results

2.1. Layered structures

In TMDs, T and H coordinations are two fundamental structural units [13]. Using these basic building blocks and considering the different stacking sequences, a bunch of crystal phases of TMDs, such as 1T, 2H, and 3R (symbols appearing in the phase nomenclature indicate the number of layers and structural stacking sequence, respectively), can be constructed. In this work, we employed 12 layered configurations to serve as the structural templates, as shown in table 1. These templates are obtained from the ICSD/Atomly database via a thorough screening process, and each of them has low energy above hull (E_{hull}), meaning they have high thermodynamic stability.

The 1T (trigonal crystal system) phase denotes the TMD structure where the monolayer with the T coordination repeats itself along the normal direction of the film, and each primitive cell contains only one monolayer sheet (three atomistic layers). It is found that transition-metal elements of group IVB, e.g. TiS_2, ZrS_2, and HfS_2, often adopt this phase [13]. 1T′ (monoclinic) and T_d (orthorhombic) phases are both referred to as twisted 1T configurations. The main difference between 1T′ and T_d phases is their crystal symmetry, since all three bond angles within the T_d structure are right angles, but one of them in 1T′ is not. These two phases can be found in 1T′-$MoTe_2$ and T_d-WTe_2, respectively [14–16]. The ReS_2-type (triclinic) phase displays a distorted configuration, and it can be regarded as a deformed 1T′ structure with even lower symmetry [17].
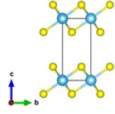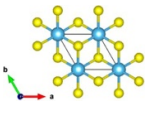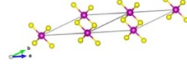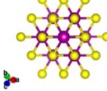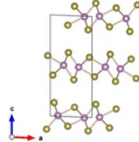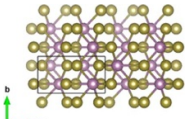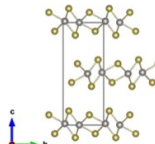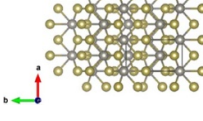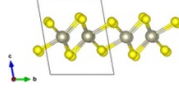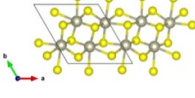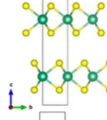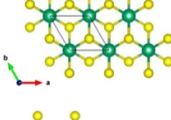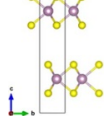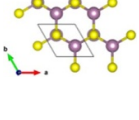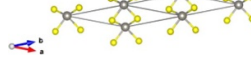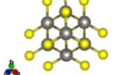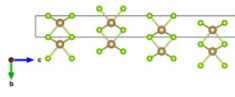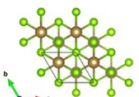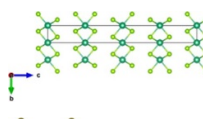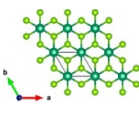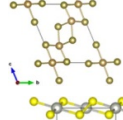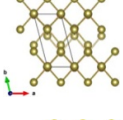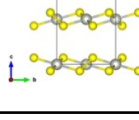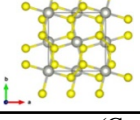
Similarly, the 2H (hexagonal) phase is fabricated by monolayers with the H coordination, where there are two monolayers in each primitive cell. Some transition-metal elements, mainly the group VB and group VIB, tend to form two types of 2H phase, e.g. 2Hc-MoS_2 and 2Ha-NbS_2 [1, 13].

The 3R (trigonal) structure is the most common phase apart from 1T and 2H. Compounds that show up with 2H phases are usually also stable in the form of 3R. Therefore, as in the case of the 2H phase, elements of group VB and VIB can generally form 3R allotropes as well [1]. There are three TX_2 layers with H coordination in each primitive cell of the 3R polytype. The MnS_2-type (trigonal) structure also exhibits a triple stacking sequence, while its monolayer displays the construction of T coordination.

The 4Ha and 4Hb are phases with four sandwich sheets within their primitive cells, both belonging to the hexagonal crystal system. All four layers in the 4Ha phase are composed of H coordination units, but for 4Hb, the T and H sheets stack over each other alternately.
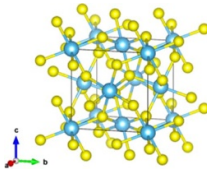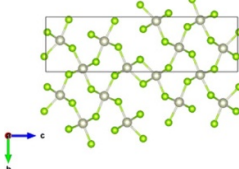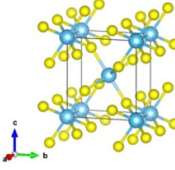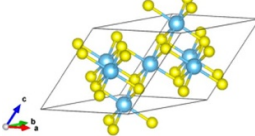
In addition, there are a number of uncommon configurations, such as the $TaTe_2$-type (monoclinic) and PdS_2-type

Table 1. Structural templates of transition metal dichalcogenides. Both the ICSD and Atomly ID numbers are provided.

Phase	Space group	IDs	Structure
1T	$P\bar{3}m1$	ICSD: 41663 Atomly: 0000085374	
MnS$_2$-type	$R\bar{3}m$	Atomly: 0000028126	
1T$'$	$P2_1/m$	ICSD: 14349 Atomly: 0000071402	
Td	$Pmn2_1$	ICSD: 14348 Atomly: 0000088534	
ReS$_2$-type	$P\bar{1}$	ICSD: 650077 Atomly: 1000297 018	
2Ha	$P6_3/mmc$	ICSD: 237033 Atomly: 0000018369	
2Hc	$P6_3/mmc$	ICSD: 49801 Atomly: 0000057650	
3R	$R3m$	ICSD: 202367 Atomly: 0000078797	
4Ha	$P6_3mc$	ICSD: 26249 Atomly: 0000090514	
4Hb	$P6_3/mmc$	ICSD: 645379 Atomly: 0000004837	
TaTe$_2$-type	$C2/m$	ICSD: 155325 Atomly: 0000046355	
PdS$_2$-type	$Pbca$	ICSD: 648753 Atomly: 0000040764	

(Continued.)

Table 1. (Continued.)

Phase	Space group	IDs	Structure
Pyrite-type	$Pa\bar{3}$	ICSD: 181501 Atomly: 0000043585	
α-RhSe$_2$-type	$Pnma$	ICSD: 650286 Atomly: 0000064531	
Marcasite-type	$Pnnm$	ICSD: 181502 Atomly: 1000146449	
Spinel-type	$Fd\bar{3}m$	ICSD: 72042 Atomly: 1000298367	

(orthorhombic) phases [1, 18]. In TaTe$_2$-type configuration, twisted Ta-Te octahedrons align themselves in a special way, which is commonly adopted by tellurides of group VB. The PdS$_2$-type (orthorhombic) structure is made up of undulating pentagons, and each pentagon is formed by three S and two Pd atoms. TMDs of group VIIIc may exist in this polymorph. Because of strong attraction between layers, PdS$_2$-type structures composed of elements other than group VIIIc will experience interlayer compression and transform into the non-layered pyrite-type phase.

2.2. Non-layered structures

Apart from layered TMDs, non-layered TX$_2$ dichalcogenides normally occur in group VIIB and beyond. For instance, marcasite (FeS$_2$) is one of the most common minerals in nature. Other four non-layered polymorphs are found from structure screening with additional structural templates, including the pyrite-type (cubic), α-RhSe$_2$-type (orthorhombic), marcasite-type (orthorhombic) and spinel-type (cubic) phases. Their information, such as the space groups, database IDs (both the ICSD and Atomly IDs) as well their atomic structures, are all shown in table 1.

2.3. Stability of the bulk TMDs (layered and non-layered)

After performing the high-throughput calculations of 1008 TMD structures (including both layered and non-layered phases), the E_{hull} for each phase can be derived (the material details can be queried from the Atomly database online).

In general, E_{hull} describes the driving force in energy to decompose a compound, and the low E_{hull} suggests good thermodynamic stability [19]. Therefore, a broad picture of the thermodynamic stability of all TMDs can be constructed.

Figure 1 shows the calculated thermodynamic stability of every possible TMDs. From this heatmap, the vertical axis presents 16 structural polytypes, and the horizontal axis denotes 21 transition metals. Each box in the figure stands for an allotrope of TMDs. Inside each box, a round disk is divided into three parts, and the upper right, the left, and the lower right parts represent the sulfide, selenide and telluride, respectively. The depth of color indicates the value of E_{hull}, where the dark blue color represents the low E_{hull}, and the yellow color means the large E_{hull}, ranging from 0 to 300 meV per atom. In each box, the TX$_2$ compound which is labeled with the light blue fan shape has been successfully synthesized in experiments, and the compound with the pink fan shape denotes a high-pressure phase in previous synthesis experiments. The empty boxes (or the missing parts of round disks) indicate that the corresponding compounds are extremely unstable as they will transform into other phases after structural optimization. The compounds that do not have the outmost fan-shaped area are the hypothetic compounds, which have not yet been experimentally produced based on our knowledge. Therefore, this figure provides an overview of the stability and synthesizability of TMDs.

Since the oxidation valence state of transition metals in layered TMDs is +4, the number of electrons on the d orbitals are d^0 for group IVB, d^1 for group VB, d^2 for group VIB, d^3 for group VIIB, d^4 for group VIIIa, d^5 for group VIIIb, and d^6 for
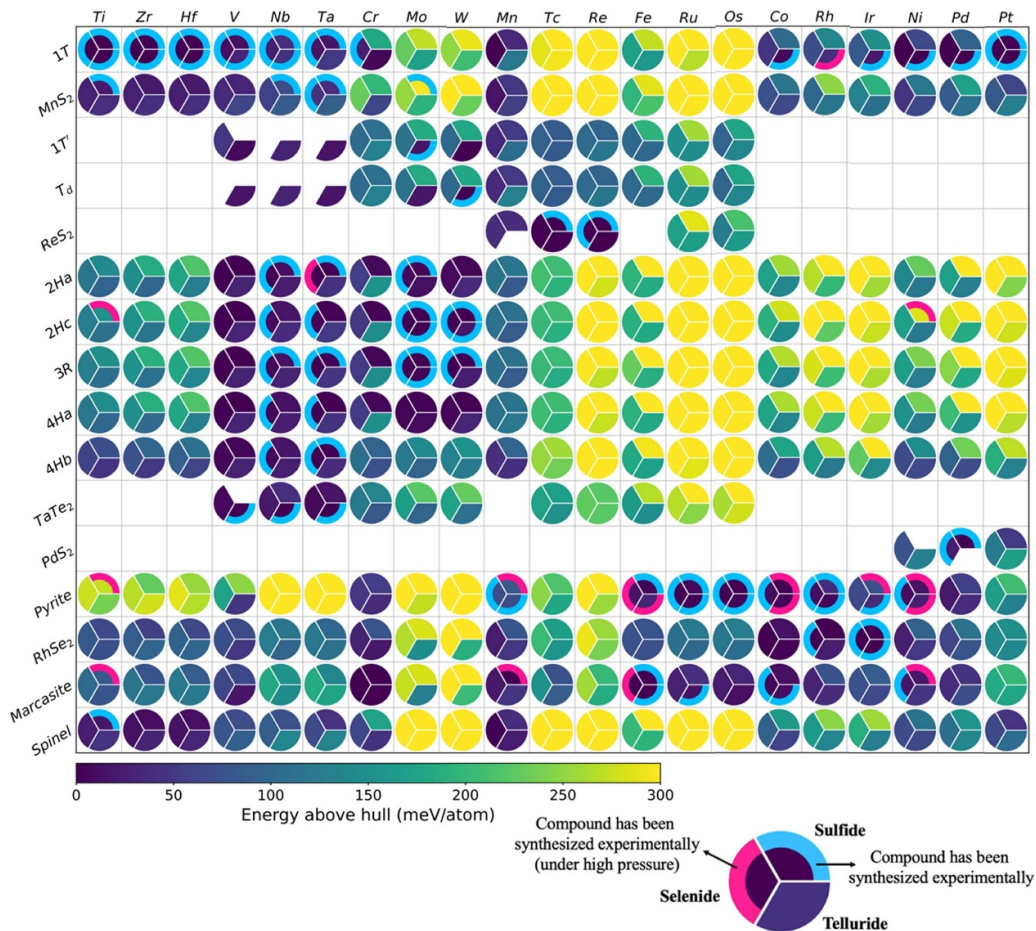
Figure 1. Thermodynamic stability of TMDs. A total of 1008 TMD compounds are calculated. Each box represents a polytype of TMDs. Inside each box, a round disk is divided into three parts, and the upper right, the left, and the lower right parts represent the sulfide, selenide and telluride, respectively. The light blue fan shapes represent that the compounds have been synthesized experimentally, and the pink fan shapes denote the high-pressure synthesis environment. The empty boxes (or the missing parts of round disks) indicate that the corresponding compounds are extremely unstable. The depth of color indicates the value of energy above hull, which can be used to quantify the thermodynamic phase stability of materials.

group VIIIc. Because the splitting and degeneracy of *d* orbitals are different under the T and H coordinations (figure S1), the number of electrons on the *d* orbitals fundamentally determines the stable phases that TMDs can adopt [20].

Among the large phase space, the 1T polytype is the most stable polymorph for all compounds of group IVB (d^0). In addition to the 1T phase, the T coordinated MnS_2-type also have high stability ($E_{hull} < 50$ meV/atom) for elements in group IVB. In contrast, only 2Hc-TiS$_2$, which belongs to the 2H phase with H coordination, has been theoretically predicted to exist under high pressure [21]. Since the energies of t_{2g} orbitals in the T coordination are higher than that of the d_{z^2} orbital in the H coordination (figure S1), the atomic structures comprising group VB (d^1) metals are inclined to adopt H coordination configurations. The results (as shown in figure 1) manifest it very well as nearly all of the most stable polytypes of group VB belong to the 2H phase. However, due to the small energy difference between the t_{2g} and d_{z^2} orbitals, the E_{hull} between 1T and 2H phases are very close, indicating that compounds of group VB can adopt both 1T and 2H polytypes. For example, the most stable polytype of VS$_2$ belongs to the

2H polymorph, but its metastable 1T phase is experimentally synthesizable (see figure 1), as the energy difference between these two phases is very small ($\sim$12 meV/atom). The thermal effect plays an important role here, and if the external environment reaches room temperature, the actual stable phase of VS$_2$ may change from the 2H to 1T polytype [13].

For compounds with 2d-electrons on each TM atom, H coordination with fully filled d_{z^2} orbital is likely the thermodynamically stable structure (figure S1). Hence the structures of group VIB (d^2) tend to choose the H coordination configurations (as shown in figure 1). In addition, the 3R phase made with the same triangular prismatic coordination as the 2H phase exhibits high stability as its E_{hull} is very small ($<$5 meV/atom), hence it may lead to the coexistence of these phases when synthesizing compounds for metal elements in this group. Indeed, it is found that experimentally synthesized 2H-type compounds of group VIB often contain 3R-type, such as the synthesis of 2H-MoS$_2$ [13].

Nearly all of the most stable phases ($E_{hull} = 0$ meV/atom) of group VIIB (d^3) are structures with twisted T coordination. For example, the ground-state polytypes of all compounds

composed of Tc and Re belong to the ReS$_2$-type phase. Electrons of compounds of group VIIIc (d^6) fully occupy their non-bonding d orbitals between the bonding and anti-bonding states. Since the non-bonding state of T coordination (mainly contributed by t_{2g} orbitals as shown in figure S1) has a lower energy than that of H coordination (mainly contributed by orbitals of d_{z^2}, $d_{x^2-y^2}$ and d_{xy} as shown in figure S1), compounds of group VIIIc tend to adopt the T coordination polytypes. Therefore, the stable structures of group VIIIc, as shown in figure 1, are mostly in the 1T phase.

For compounds in group VIIB and VIII, non-layered phases are thermodynamically more stable. Due to the absence of van der Waals interlayer spacing, their bonding behavior is completely different from those of layered ones, while the basic building block is still the T coordination construction. For compounds of Fe, marcasite- and pyrite-type are the most common polytypes. According to our calculations, marcasite- and pyrite-type FeX$_2$ (X = S, Se, Te) are the two compounds with high thermodynamic stability (E_{hull} < 30 meV/atom), and it agrees with the experiments very well as they are synthesizable [22, 23]. The pyrite-type MnX$_2$ (X = S, Se, Te) compounds are less stable ($E_{hull} \cong 70$ meV/atom) than their marcasite- and spinel-type counterparts ($E_{hull} \cong 40$ meV/atom), but they are still experimentally synthesizable according to their moderate E_{hull} [24, 25]. RhSe$_2$-type is the most stable phase among all the compounds of Rh and Ir. From figure 1, elements in other groups may also adopt this configuration (MnSe$_2$, CrSe$_2$, CrTe$_2$, and NiSe$_2$, etc.). PdS$_2$-type has a unique configuration, as it can be viewed as the pyrite-type structure with prominently stretched M–X bonds due to the 'Jahn-Teller effect', therefore it is feasible to have PdS$_2$-type to pyrite-type phase transition under high pressure, in which the van der Waals interlayer spacing is squeezed away [26]. The PdS$_2$-type phase only exists in group VIIIc (as shown in figure 1). In addition to the experimentally synthesizable PdS$_2$-type compounds (PdS$_2$ and PdSe$_2$), NiSe$_2$ and PtS$_2$ may also adopt this polytype due to their moderate thermodynamic stability (their E_{hull} equal 75 and 52 meV/atom, respectively), thus they are worth further experimental confirmation.

We have compared our calculations with the existing theories and experiments, and the results are generally in good agreement, assuring the reliability of our results. It has been observed that not only compounds with E_{hull} = 0 would exist, but also compounds with relatively small E_{hull} (generally smaller than 50 meV/atom, see table S1 for the complete list) may be potentially synthesized. It is found that there are still many potential structures with considerably good stability in TMDs awaiting for the further exploration in experiments.

2.4. Stability of the monolayer TMDs

The layered TMDs as shown in section 2.1 are composed of single-layer sandwich atom sheets, and there are only six distinctive monolayer polytypes: ML-T (space group: $P\bar{3}m1$), ML-H ($P\bar{6}m2$), ML-T′ ($P2_1/m$), ML-TaTe$_2$-type ($C2/m$), ML-ReS$_2$-type ($P\bar{1}$) and ML-PdS$_2$-type ($P2_1/c$). Detailed information and structural configurations of them are listed in table 2.
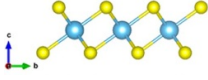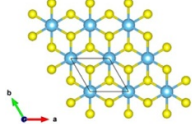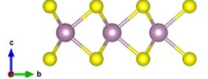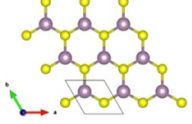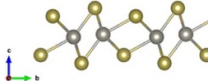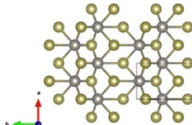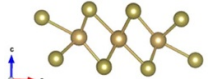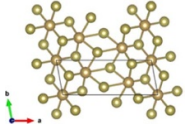
Figure 2 shows a relative energy landscape of the monolayer TMDs as the function of the polytypes and the transition metals. The color scheme of this figure represents the relative energy by using the lowest energy among the six monolayer phases in each composition space as the referenced state (not the E_{hull} used in figure 1). Figure 2 represents the relative stability of the monolayer TMDs and shows the competition in-between phases if they can be made in monolayers. Besides the energy reference, the plotting conventions similar to that in figure 1 are adopted in figure 2. Each round shape is split into three parts for the three anion species, and the depth of color denotes the magnitude of the relative energy (the darker the color, the lower the relative energy). Labels of blue arc denote that the single-layer compounds have been synthesized experimentally [27].

Similar to the bulk compounds, the number of electrons on the d orbitals determines the most stable polytypes of monolayer TMDs as well. The type of anion and the dimension of material have little effect on this structural selection principle. Compared to figure 1, we found that due to the absence of van der Waals interlayer interaction, the stability of several compounds varies. For example, TaTe$_2$-type is the most stable phase for bulk VTe$_2$. However, for monolayer VTe$_2$, ML-T′ polymorph is the most stable phase (exhibiting the lowest energy). The bulk NiS$_2$ does not exist in the PdS$_2$-type phase, since the structure will be compressed into a non-layered pyrite-type. But when the system is restricted to monolayer, NiS$_2$ in the ML-PdS$_2$-type phase, on the contrary, has the lowest energy. Previous literature demonstrated that the NiS$_2$ with the ML-PdS$_2$-type phase can be used as flexible water splitting photocatalysts within visible and ultraviolet light regions [28], hence ML-PdS$_2$-type NiS$_2$ is worth exploring experimentally as both our results and the existing work suggest its good stability. Similarly, compounds of group VIIIb do not exist as layered 1T′ and TaTe$_2$-type, but they may maintain good thermodynamic stability when they adopt the ML-T′ and ML-TaTe$_2$-type phases. For bulk compounds of group VIIB and beyond, although most of their ground-state structures belong to non-layered polymorphs, the 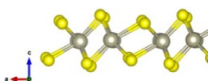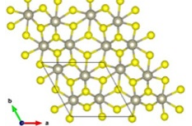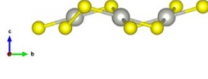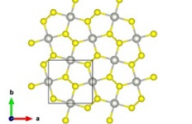existence of several monolayer compounds of these groups have been theoretically predicted, such as ML-T FeS$_2$ and MnS$_2$ [29, 30], which is also consistent with our results (both ML-T FeS$_2$ and MnS$_2$ have low relative energies). We list all the single-layer TMDs with relative energies below 50 meV/atom in table S2. It should be noted that kinetics is also crucial for justifying the synthesizability of a compound, which is not addressed in this paper as it is beyond the scope of the paper. Table S3 in supporting information lists the dynamic stability (based on phonon dispersions) of several compounds from the C2DB database [31], which shows that the thermodynamic stability primarily determines the synthesizability, and the dynamic stability should also be considered as an important factor as well.

2.5. Exfoliation energy of layered TMDs

After performing the first-principles calculations on both layered and monolayer TMDs, their exfoliation energies can be derived easily. As shown in figure 3, exfoliation energies

Table 2. Structural templates of monolayer TMDs. All the IDs are from the Atomly database.

Phase	Space group	IDs	Structure	
ML-T	$P\bar{3}m1$	Atomly: 1000002533		
ML-H	$P\bar{6}m2$	Atomly: 1000002671		
ML-T′	$P2_1/m$	Atomly: 1000002613		
ML-TaTe$_2$-type	$C2/m$	Atomly: 1000298647		
ML-ReS$_2$-type	$P\bar{1}$	Atomly: 1000298600		
ML-PdS$_2$-type	$P2_1/c$	Atomly: 1000002897		
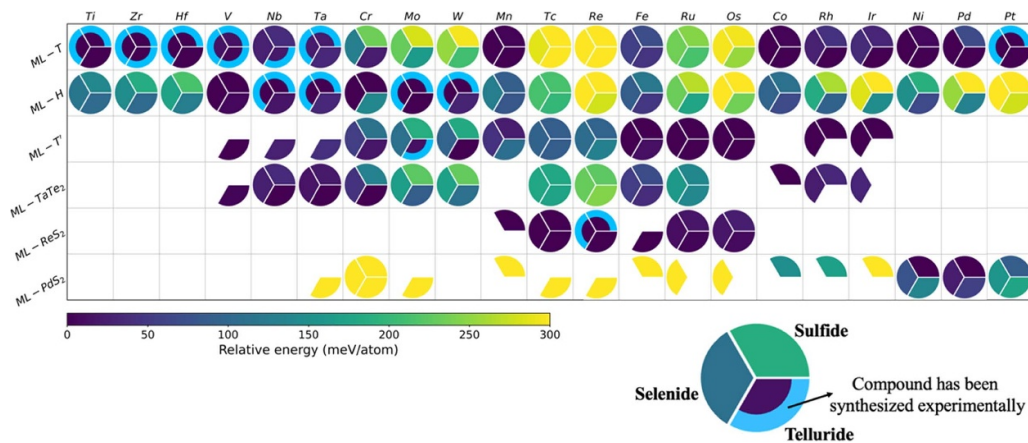
Figure 2. The relative energy of monolayer TMDs. A total of 378 single-layer TMD compounds are calculated. The depth of color represents the relative energy in each composition space. Labels of blue arc denote that the single-layer compounds have been synthesized experimentally. Other plotting details are similar to figure 1.

of 756 layered configurations are obtained [32, 33]. The plotting methods are similar to figure 1. The size of each sector stands for the likelihood of the existence of the corresponding compound, which is inversely proportional to the magnitude of E_{hull} of the compound. For each one-third fraction of disk, the depth of color represents the magnitude of exfoliation energy (E_{exf}), and the orange arc denotes that the corresponding layered compound has been experimentally verified its exfoliability by the top-down method (mechanical or liquid-phase exfoliation) [27].
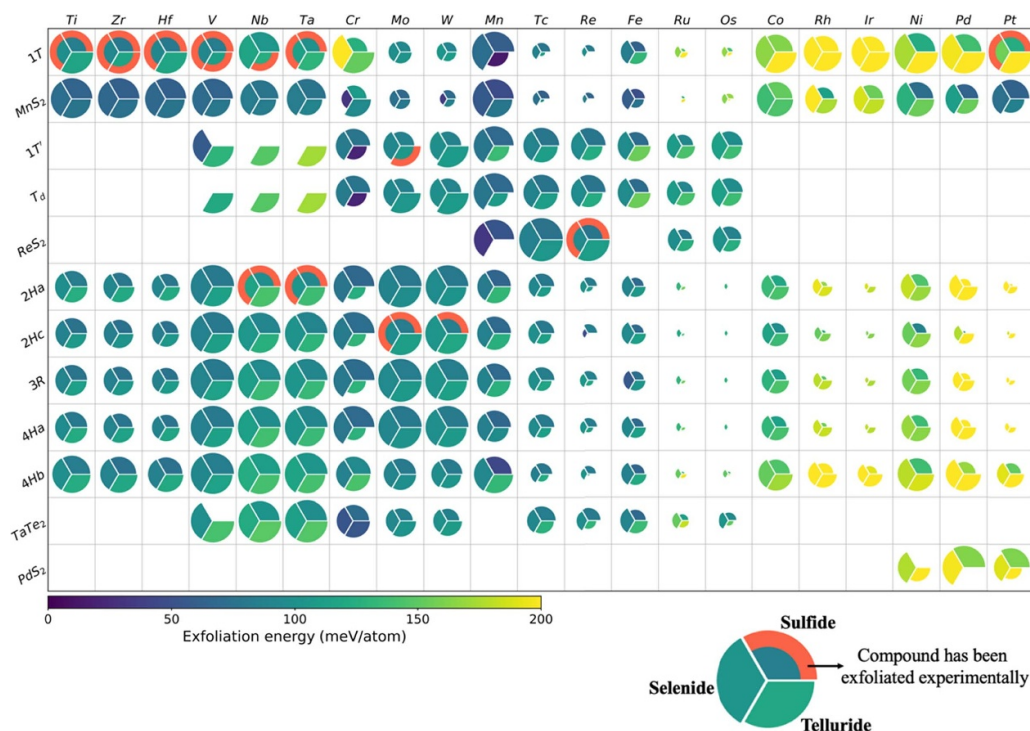
Figure 3. Exfoliation energy of layered TMDs. A total of 756 layered TMD compounds are calculated. The size of each sector represents the likelihood of the existence of the corresponding compounds (the size is inverse proportional to the thermodynamic stability). The depth of color represents the magnitude of exfoliation energy and the orange arc denotes that the layered material has been experimentally verified its exfoliability. Other plotting details are similar to figure 1.

Generally speaking, the existence of free-standing single-layered TMDs is warranted only when the van der Waals interaction between layers is weak (or the exfoliation energy is low enough) [33, 34]. As revealed in previous studies, layered materials with E_{exf} of less than 150 meV/atom are exfoliable [33, 35]. Herein, we employed both the E_{exf} and the E_{hull} to determine the synthesizability of the free-standing single-layer TMDs. In this work, we classified layered TMDs into four categories: 'easily exfoliable' (EE) for $E_{exf} < 100$ meV/atom and $E_{hull} < 50$ meV/atom; 'feasibly exfoliable' (FE) for 100 meV/atom $< E_{exf} < 150$ meV/atom and $E_{hull} < 50$ meV/atom; 'potentially exfoliable' (PE) for $E_{exf} < 150$ meV/atom and 50 meV/atom $< E_{hull} < 100$ meV/atom; and 'non-exfoliable' (NE) for the rest. By applying chemical or mechanical exfoliation methods, several layered TMDs have been successfully exfoliated into monolayers, such as 2Ha-NbSe$_2$, 1T-NbTe$_2$, 2Ha-TaS$_2$, 2Ha-TaSe$_2$, 1T'-MoTe$_2$, 1T-TaS$_2$, 1T-TiS$_2$ and 2Hc-MoS$_2$, etc [3, 36]. Those compounds all belong to the 'EE' or 'FE' category of TMDs as we defined above, validating the accuracy of our calculations. The complete classification is shown in table S4. It is worth noting that compounds with large E_{hull} usually have descended E_{exf} since the unstable compounds tend to break down to other polymorphs and the monolayer phases may improve their thermodynamic stability. For example, 2Ha-TiS$_2$ has an appropriate E_{exf} of 85 meV/atom, but it is highly unstable ($E_{hull} = 142$ meV/atom).

3. Discussion

It is well known that the number of electrons filling in the non-bonding *d* orbitals determines not only the stable configurations but also the electronic structures of TMDs [20]. The non-bonding *d* orbitals of group IVB (d^0) and group VIIIc (d^6) are unoccupied and fully occupied, respectively. Thus, compounds of group IVB and VIIIc are semiconductors in theory. Compounds of group VB (d^1) are metals no matter whether they are T or H coordination phases. Besides, for H coordination structures in group VB, electrons half-fill d_{z^2} orbitals, resulting in narrow-band metals. In contrary, d_{z^2} orbitals of compounds of group VIB (d^2) are fully occupied, so structures with H coordination in this group are semiconductors instead. In addition to the *d*-electron occupancy of transition metal, structural distortion is another factor that has a significant impact on the electronic states of TMDs.

The driving force behind structural distortions is known as the 'Jahn-Teller effect'. Structural distortions will introduce splitting of the originally degenerate *d* orbitals, further changing the arrangement of electrons and thus affecting the electronic structures of TMDs. A representative example is the PdS$_2$-type mentioned in section 2.3, which is obtained by the occurrence of 'Jahn-Teller distortion' in pyrite-type structure [26]. According to our calculations, both pyrite- and PdS$_2$-type NiSe$_2$ have moderate stability (E_{hull} equal 11 and 75 meV/atom, respectively). As shown in figure S2, for each
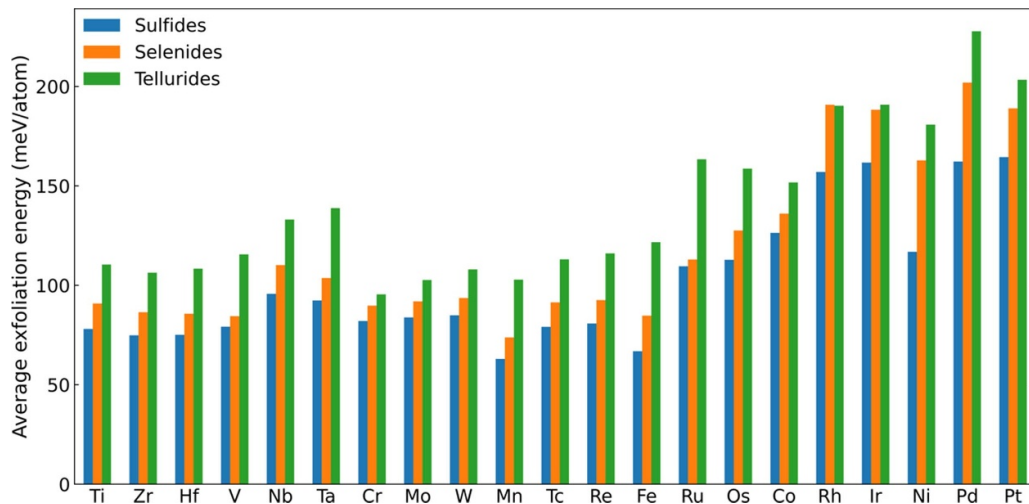
Figure 4. Average exfoliation energies versus transition metals for different anionic environments.

octahedron within the pyrite-type $NiSe_2$, stretching two opposite T–X bonds (along the *z*-axis) yields the PdS_2-type phase. Due to the 'Jahn-Teller distortion', the two degenerate e_g orbitals ($d_{x^2-y^2}$, d_{z^2}) of the compound split, and the energy of the d_{z^2} orbital drops, thus both electrons transfer from their original position, e_g to d_{z^2}. Consequently, $NiSe_2$ changes from a metal to a semiconductor.

Compared with deformations in non-layered pyrite-type compounds, structural distortions in layered or monolayer TMDs will bring a rich variety of physical phenomena. The structural distortions that occur in the pyrite-type $NiSe_2$ only involve the stretching and shrinking of bonds. In layered TMDs, transition metal at the center of the octahedron will shift away from its high-symmetry centric position, which not only causes the expansion and contraction of bond lengths but also changes bond angles. This highly distorted six-coordinated configuration may change the degeneracy of *d* orbitals and significantly alter the electronic states of TMDs. For example, the t_{2g} orbitals of ML-T MoS_2 are one-third occupied, which results in a completely metallic state. After lattice distortion, there will be a band inversion near the Fermi surface, and MoS_2 turns into a semiconductor with the ML-1T′ polytype instead [37]. When transition metal deviates too far from the central site of T coordination, it may cause interactions among adjacent metal atoms, resulting in metal–metal bonding. Therefore, such structural distortions in TMDs cause not only cleavage of degenerated *d*-orbitals, but also the establishment of some filled sub-bands due to metal–metal bonding [1]. For instance, ReS_2-type MnS_2 is a distorted structure with good thermodynamic stability ($E_{hull} = 38$ meV/atom) and has three non-bonding electrons. Thus, MnS_2 would be metal in regular T coordination. In fact, the partially filled non-bonding orbitals (t_{2g} orbitals) are converted into fully filled metal–metal bonding orbitals due to Mn atoms clustering into a unit of four Mn atoms, leading to the transition of MnS_2 from the metallic state with the 1T phase to the semiconductor state with the ReS_2-type. Statistics on the structural distortions in TMDs can be found in table S5.

The *d*-electron count of transition metals in TMDs largely determines configurations and electronic states of materials, so what role do the different chalcogen anions play in TMDs? For each X-T-X sandwich sheet in layered TMDs, the accumulated charge in its two chalcogen planes will cause Coulomb repulsion among layers [38]. Due to the formation of ionic bondings with transition metals, chalcogen anions with greater electronegativity will accumulate more charges. Thus, it is foreseeable that the exfoliation energies of layered TMDs are related to the electronegativity of chalcogen anions: the greater the electronegativity, the smaller the exfoliation energy. As shown in figure 4, for each transition metal, we calculated its three average exfoliation energies under different anionic environments (S, Se, Te). It can be observed that the average exfoliation energy for each transition metal decreases from tellurides and selenides to sulfides, which is consistent with the decreasing trend of the electronegativity of S, Se, Te (2.58, 2.55 and 2.11 [39], respectively). Therefore, S anions are expected to accept more electrons than Se and Te, leading to the strongest Coulomb repulsion among layers. Hence, sulfides are generally easier to be exfoliated than corresponding selenides and tellurides.

4. Conclusions

Combining transition metals (from group IVB to VIIIc) with three chalcogens (S, Se, Te) in different polymorphic phases, we investigated 1008 bulk and 378 monolayer TMDs. Aided by the high-throughput first-principles calculations and available materials database, we constructed comprehensive thermodynamic and exfoliation-energy landscapes to quantitatively justify the structural stability as well as the exfoliability of TMDs. It is found that the experimentally synthesizable compounds all have small E_{hull}, validating the accuracy of the state-of-the-art, systematic first-principles calculations. VSe_2 in 1T′ phase, VTe_2 in T_d phase and $TaTe_2$ in T_d phase are predicted to have high thermodynamic stability, hence they are

likely to be synthesized in near future and are highly recommended for further exploration. In monolayer TMDs, ML-T′ VSe$_2$ and ML-ReS$_2$-type MnS$_2$ have the best chance to be made experimentally according to their combined merit of stability and exfoliability. The occupation state of non-bonding d orbitals of transition metals determines both the stable polytypes and electronic structures of TMDs. Structural distortion is another key factor that strongly affects the electronic properties of TMDs as well (ReS$_2$-type MnS$_2$, etc.). It is found that, due to the gradually decreasing electronegativity of S, Se, Te, the E_{exf} of sulfide, selenide and telluride increase progressively. It is our hope that this work will provide useful guidance for further discovery and synthesis of TMDs for their potential wide applications in science and technology.

5. Methods

The DFT calculations were carried out under the generalized gradient approximation for the exchange correlation potential as proposed by Perdew–Burke–Ernzerhof (PBE) [40]. The semi-local function such as PBE lacks the ability to properly describe the weak interlayer van der Waals interactions of layered crystals such as TMDs. For that matter, we considered the vdW-D3 correction to improve the description of the layered structures [41]. Based on the Vienna *Ab initio* Simulation Package [42], Gaussian smearing method (ISMEAR = 0), a cutoff energy of 520 eV, a gamma-centered k-mesh, and the k-point density of at least 3000/(number of atoms in the cell) were used for all the calculations (tetrahedron smearing method with ISMEAR = −5 for density of states calculations). A total energy convergence criterion of 10^{-5} eV was employed for the self-consistent cycle, and equilibrium volumes were obtained once the change of the total energy between two ionic steps were less than 10^{-4} eV. For structural optimizations, the volume, shape and coordinates of atoms of $1 \times 1 \times 1$ supercell were all allowed to be relaxed. For single-layer materials, a spacing of 20 Å between layers was used to prevent the layers from interacting with each other. All the calculations are conducted in a high-throughput mode by employing the workflow and database of atomly.net materials science data infrastructure.

To evaluate the thermodynamic stability of a compound, we constructed a convex hull in the corresponding chemical space with the help of the Atomly materials database. Once the convex hull is constructed, the distance of the compound to the convex hull is defined as the energy above hull (E_{hull}). We used the pymatgen package to construct the phase diagrams and calculate the E_{hull} of compounds [43].

Exfoliation energy (E_{exf}) is defined as:

$$E_{exf} = \frac{E_L}{N_L} - \frac{E_{ML}}{N_{ML}}$$

where E_L is the energy of the layered structure, N_L is the atomic number of the layered structure, E_{ML} is the energy of the monolayer structure, and N_{ML} is the atomic number of the monolayer structure.

ORCID iDs

Tenglong Lu ⬡ https://orcid.org/0000-0003-0670-4036
Huaxian Jia ⬡ https://orcid.org/0000-0002-3586-0225
Miao Liu ⬡ https://orcid.org/0000-0002-1843-9519

References

[1] Wilson J A and Yoffe A D 1969 The transition metal dichalcogenides discussion and interpretation of the observed optical, electrical and structural properties *Adv. Phys.* **18** 193–335
[2] Nicolosi V, Chhowalla M, Kanatzidis M G, Strano M S and Coleman J N 2013 Liquid exfoliation of layered materials *Science* **340** 1226419
[3] Li J *et al* 2021 Printable two-dimensional superconducting monolayers *Nat. Mater.* **20** 181–7
[4] Splendiani A, Sun L, Zhang Y, Li T, Kim J, Chim C Y, Galli G and Wang F 2010 Emerging photoluminescence in monolayer MoS$_2$ *Nano Lett.* **10** 1271–5
[5] Xiao D, Liu G B, Feng W, Xu X and Yao W 2012 Coupled spin and valley physics in monolayers of MoS$_2$ and other group-VI dichalcogenides *Phys. Rev. Lett.* **108** 196802
[6] Bhandavat R, David L and Singh G 2012 Synthesis of surface-functionalized WS$_2$ nanosheets and performance as Li-ion battery anodes *J. Phys. Chem. Lett.* **3** 1523–30
[7] Liu C, Chen H, Wang S, Liu Q, Jiang Y-G, Zhang D W, Liu M and Zhou P 2020 Two-dimensional materials for next-generation computing technologies *Nat. Nanotechnol.* **15** 545–57
[8] Liu Z, Na G, Tian F, Yu L, Li J and Zhang L 2020 Computational functionality-driven design of semiconductors for optoelectronic applications *InfoMat* **2** 879–904
[9] Lu X-C, Lu Y-Z, Wang C and Cao Y 2022 Efficient photoelectrodes based on two-dimensional transition metal dichalcogenides heterostructures: from design to construction *Rare Met.* **41** 1142–59
[10] Niu H, Wang X, Shao C, Zhang Z and Guo Y 2020 Computational screening single-atom catalysts supported on g-CN for N$_2$ reduction: high activity and selectivity *ACS Sustain. Chem. Eng.* **8** 13749–58
[11] Belsky A, Hellenbrandt M, Karen V L and Luksch P 2002 New developments in the Inorganic Crystal Structure Database (ICSD): accessibility in support of materials research and design *Acta Crystallogr.* B **58** 364–9
[12] Atomly Materials Database (available at: www.atomly.net)
[13] Chhowalla M, Shin H S, Eda G, Li L J, Loh K P and Zhang H 2013 The chemistry of two-dimensional layered transition metal dichalcogenide nanosheets *Nat. Chem.* **5** 263–75
[14] Keum D H *et al* 2015 Bandgap opening in few-layered monoclinic MoTe$_2$ *Nat. Phys.* **11** 482–6
[15] Cho S *et al* 2015 Phase patterning for ohmic homojunction contact in MoTe$_2$ *Science* **349** 625–8

[16] Lee C-H, Silva E C, Calderin L, Nguyen M A T, Hollander M J, Bersch B, Mallouk T E and Robinson J A 2015 Tungsten ditelluride: a layered semimetal *Sci. Rep.* **5** 10013

[17] Saha P, Ghosh B, Mazumder A, Glazyrin K and Dev Mukherjee G 2020 Pressure induced lattice expansion and phonon softening in layered ReS$_2$ *J. Appl. Phys.* **128** 085904

[18] Wang Y, Li Y and Chen Z 2015 Not your familiar two dimensional transition metal disulfide: structural and electronic properties of the PdS$_2$ monolayer *J. Mater. Chem.* C **3** 9603–8

[19] Sun W, Dacek S T, Ong S P, Hautier G, Jain A, Richards W D, Gamst A C, Persson K A and Ceder G 2016 The thermodynamic scale of inorganic crystalline metastability *Sci. Adv.* **2** e1600225

[20] Yang H, Kim S W, Chhowalla M and Lee Y H 2017 Structural and quantum-state phase transitions in van der Waals layered materials *Nat. Phys.* **13** 931–7

[21] Yu Y G and Ross N L 2011 First-principles study on thermodynamic properties and phase transitions in TiS$_2$ *J. Phys.: Condens. Matter* **23** 055401

[22] Brostigen G and Kjekshus A 1970 Compounds with the marcasite type crystal structure *Acta Chem. Scand.* **24** 1925–40

[23] Bither T A, Bouchard R J, Cloud W H, Donohue P C and Siemons W J 1968 Transition metal pyrite dichalcogenides high-pressure synthesis and correlation of properties *Inorg. Chem.* **7** 2208–20

[24] Kimber S A, Salamat A, Evans S R, Jeschke H O, Muthukumar K, Tomić M, Salvat-Pujol F, Valentí R, Kaisheva M V and Zizak I 2014 Giant pressure-induced volume collapse in the pyrite mineral MnS$_2$ *Proc. Natl Acad. Sci.* **111** 5106–10

[25] Elliott N 1937 The crystal structure of manganese diselenide and manganese ditelluride *J. Am. Chem. Soc.* **59** 1958–62

[26] Soulard C, Rocquefelte X, Petit P E, Evain M, Jobic S, Itié J P, Munsch P, Koo H J and Whangbo M H 2004 Experimental and theoretical investigation on the relative stability of the PdS$_2$- and pyrite-type structures of PdSe$_2$ *Inorg. Chem.* **43** 1943–9

[27] Wang Q H, Kalantar-Zadeh K, Kis A, Coleman J N and Strano M S 2012 Electronics and optoelectronics of two-dimensional transition metal dichalcogenides *Nat. Nanotechnol.* **7** 699–712

[28] Wang C T and Du S 2020 A unique pentagonal network structure of the NiS$_2$ monolayer with high stability and a tunable bandgap *Phys. Chem. Chem. Phys.* **22** 7483–8

[29] Zhang H, Dai Y-M and Liu L-M 2015 Novel monolayer pyrite FeS2 with atomic-thickness for magnetic devices *Comput. Mater. Sci.* **101** 255–9

[30] Kan M, Adhikari S and Sun Q 2014 Ferromagnetism in MnX$_2$ (X = S, Se) monolayers *Phys. Chem. Chem. Phys.* **16** 4990

[31] Gjerding M N *et al* 2021 Recent progress of the computational 2D materials database (C2DB) *2D Mater.* **8** 044002

[32] Bjorkman T, Gulans A, Krasheninnikov A V and Nieminen R M 2012 van der Waals bonding in layered compounds from advanced density-functional first-principles calculations *Phys. Rev. Lett.* **108** 235502

[33] Revard B C, Tipton W W, Yesypenko A and Hennig R G 2016 Grand-canonical evolutionary algorithm for the prediction of two-dimensional materials *Phys. Rev.* B **93** 054117

[34] Mounet N *et al* 2018 Two-dimensional materials from high-throughput computational exfoliation of experimentally known compounds *Nat. Nanotechnol.* **13** 246–52

[35] Ashton M, Paul J, Sinnott S B and Hennig R G 2017 Topology-scaling identification of layered solids and stable exfoliated 2D materials *Phys. Rev. Lett.* **118** 106101

[36] Zeng Z, Yin Z, Huang X, Li H, He Q, Lu G, Boey F and Zhang H 2011 Single-layer semiconducting nanosheets: high-yield preparation and device fabrication *Angew. Chem., Int. Ed. Engl.* **50** 11093–7

[37] Qian X, Liu J, Fu L and Li J 2014 Quantum spin Hall effect in two-dimensional transition metal dichalcogenides *Science* **346** 1344–7

[38] Bastos C M O, Besse R, Da Silva J L F and Sipahi G M 2019 *Ab initio* investigation of structural stability and exfoliation energies in transition metal dichalcogenides based on Ti-, V-, and Mo-group elements *Phys. Rev. Mater.* **3** 044002

[39] Pauling L 1932 The nature of the chemical bond IV. The energy of single bonds and the relative electronegativity of atoms *J. Am. Chem. Soc.* **54** 3570–82

[40] Perdew J P, Burke K and Ernzerhof M 1996 Generalized gradient approximation made simple *Phys. Rev. Lett.* **77** 3865–8

[41] Grimme S, Antony J, Ehrlich S and Krieg H 2010 A consistent and accurate *ab initio* parametrization of density functional dispersion correction (DFT-D) for the 94 elements H-Pu *J. Chem. Phys.* **132** 154104

[42] Kresse G and Furthmüller J 1996 Efficient iterative schemes for *ab initio* total-energy calculations using a plane-wave basis set *Phys. Rev.* B **54** 11169–86

[43] Ong S P, Richards W D, Jain A, Hautier G, Kocher M, Cholia S, Gunter D, Chevrier V L, Persson K A and Ceder G 2013 Python materials genomics (pymatgen): a robust, open-source Python library for materials analysis *Comput. Mater. Sci.* **68** 314–9